www.czasopisma.pan.pl PAN www.journals.pan.pl

Opto-Electronics Review 25 (2017) 274–284

Contents lists available at ScienceDirect

Opto-Electronics Review

journal homepage: http://www.journals.elsevier.com/opto-electronics review

Searching of new, cheap, air- and thermally stable hole transporting materials for perovskite solar cells

K. Gawlinska [a,*], A. Iwan [b,*], Z. Starowicz [a], Grazyna Kulesza-Matlak [a], K. Stan-Glowinska [a], M. Janusz [a], M. Lipinski [a], B. Boharewicz [c], I. Tazbir [c], A. Sikora [c]

[a] Institute of Metallurgy and Materials Science, Polish Academy of Sciences, ul. Reymonta 25, 30-059 Krakow, Poland
[b] Military Institute of Engineer Technology, ul. Obornicka 136, 50-961 Wroclaw, Poland
[c] Electrotechnical Institute, Division of Electrotechnology and Materials Science, ul. M. Sklodowskiej-Curie 55/61, 50-369 Wroclaw, Poland

ARTICLE INFO

Article history:
Received 16 January 2017
Received in revised form 31 May 2017
Accepted 27 July 2017
Available online 22 September 2017

Keywords:
Perovskite
Polyazomethines
Solar cells
Photovoltaics

ABSTRACT

In this work, two thermal- and air-stable, hole transporting materials (HTM) in perovskite solar cells are analyzed. Those obtained and investigated materials were two polyazomethines: the first one with three thiophene rings and 3,3′-dimethoxybenzidine moieties (S9) and the second one with three thiophene rings and fluorene moieties (S7). Furthermore, presented polyazomethines were characterized by Fourier transform infrared spectroscopy (FTIR), UV–vis spectroscopy, atomic force microscopy (AFM) and thermogravimetric analysis (TGA) experiments. Both polyazomethines (S7 and S9) possessed good thermal stability with a 5% weight loss at 406 and 377 °C, respectively. The conductivity of S7 was two orders of magnitude higher than for S9 polymer (2.7×10^{-8} S/cm, and 2.6×10^{-10} S/cm, respectively). Moreover, polyazomethine S9 exhibited 31 nm bathochromic shift of the absorption band maximum compared to S7.

Obtained perovskite was investigated by UV–vis and XRD. Electrical parameters of perovskite solar cells (PSC) were investigated at Standard Test Conditions (STC). It was found that both polyazomethines protect perovskite which is confirmed by ageing test where V_{oc} did not decrease significantly for solar cells with HTM in contrast to solar cell without hole conductor, where V_{oc} decrease was substantial. The best photoconversion efficiency (PCE = 6.9%), among two investigated in this work polyazomethines, was obtained for device with the following architectures FTO/TiO_2/TiO_2 + perovskite/S7/Au. Stability test proved the procreative effects of polyazomethines on perovskite absorber.

1. Introduction

Recently, perovskites solar cells have been an extremely hot topic in a photovoltaic world due to their excellent optical and electrical properties. General formula of hybrid perovskite is ABX_3, where B is a bivalent cation such as lead (Pb^{2+}) or tin (Sn^{2+}), X is an anion, usually halide ion, for example chloride (Cl^-), iodide (I^-) or bromide (Br^-) while A is an organic cation as methylammonium ($CH_3NH_3^+$) or formamidinium ($NH=CHNH_3$) [1]. The crystal structure of perovskite consist of a corner sharing (BX6) octahedron where cation B is located in the centre while anion X in the corners. The biggest cation A is situated between the octahedrons and its main issue is to balance a perovskite structure [2]. The archetype of perovskite solar cells are Dye Sensitized Solar Cells (DSSC) which contain mesoporous TiO_2 covered by organic, dye molecules, for which operating principle is given by Anders Hagfeldt and Michael Grätzel [3]. The parameters which make perovskite attractive to photovoltaic purposes are optimal band-gap energy which is equal to 1.5 eV–1.8 eV, low exciton binding energy, relatively high carrier lifetime (even 100 ns) compared with organic solar cells (10 ns) and high diffusion length of 100–1000 nm, depending on the compound composition [4]. Moreover, perovskites have low non-radiative recombination rates losses compared to other thin-film polycrystalline semiconductors [5].

Main disadvantages to be mentioned are, low ambient stability and UV light, oxygen and moisture sensitivity [6]. Furthermore, manufacturing of perovskite solar devices requires very expensive components. While, perovskite material itself is rather cheap, the most common, p-type hole transporter (Spiro-OMeTAD) is even several times more expensive than gold or platinum [7]. Perfect HTM should possess high hole mobility, energy levels aligned to

* Corresponding authors.
E-mail addresses:
k.gawlinska@imim.pl (K. Gawlinska), iwan@witi.wroc.pl (A. Iwan)

http://dx.doi.org/10.1016/j.opelre.2017.07.004
1896-3757/

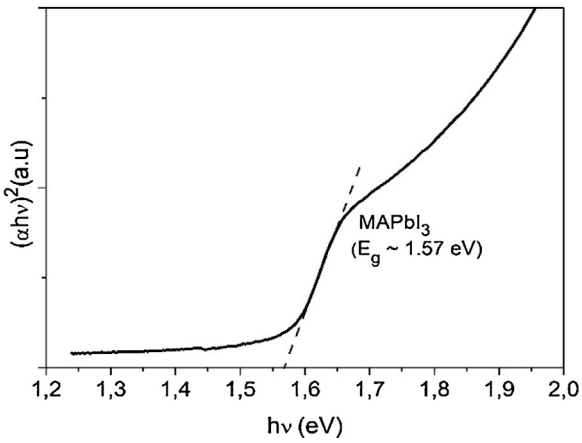

Fig. 1. Illustration of bang gap energy determination of perovskite obtained in a two step deposition method.

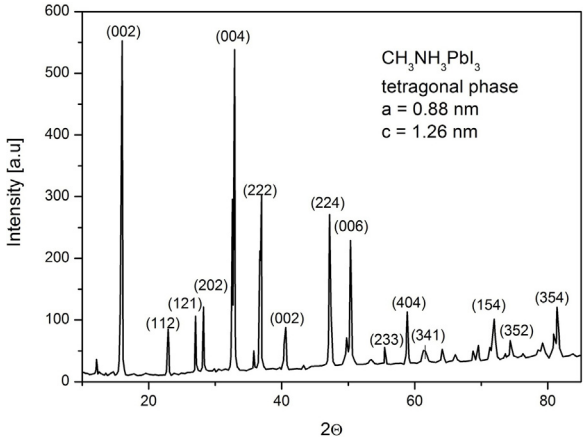

Fig. 2. X-ray diffraction pattern of perovskite powder.

the other structure components: HOMO and LUMO levels of HTM should be accordingly higher and lower than valence and conduction band of perovskite, and do not damage the perovskite itself [8]. Moreover, it shall be hydrophobic and therefore, remains stable protection and encapsulation barrier for the perovskite layer [9,10]. Basically, organic and inorganic hole transporting materials can be distinguished.

The most common organic hole transporting material is 2,2′,7,7′-tetrakis-(*N*,*N*-di-p-methoxyphenylamine)-9,9′-spirobifluorene (Spiro-OMeTAD) and it is highly successful because of its large hole mobility and high solubility [9]. Nevertheless, Spiro-OMeTAD contains LiTFSi (bis(trifluoromethane)sulfonimide lithium salt) dopant which is sensitive to humidity and leads to poor stability of perovskite solar cells [8]. Besides that, Spiro-OMeTAD is very expensive due to complicated synthesis and high purity requirement [11]. This is the main reason why many research groups try to obtain cheaper HTM by modifying this compound. As a result, such examples as spiro-cyclopenta[2,1-b:3,4-b] dithiophene (spiro-CPDT), tetra{4-[*N*,*N*-(4,4-dimethoxydiphenylamino)]phenyl}ethane(TAE-1) [9] or Trux-OMeTAD which consists of a C3h Truxene-core with arylamine terminals and hexyl side-chains, can be found [10].

On the other hand poly(3,4-ethylenedioxythiophene)-poly(styrenesulfonate) (PEDOT:PSS) is cheap polymer with high conductivity. Typically, PEDOT:PSS applied as an HTM layer in inverted structure and it is usually located on the top of devices. Nonetheless, sometimes it can provide a part of a scaffold structure but in such a case it is very important to be aware of destructive influence of water on perovskite. Therefore, the PEDOT:PSS in toluene solution has to be used instead of aqua dilution. Liu et al. have shown that PEDOT:PSS has similar properties as Spiro-OMeTAD [8]. Moreover, it is possible to control conductivity of PEDOT by dopant changing [12]. Small amount of PSS improves conductivity simultaneously increasing the charge carrier mobility and therefore, better electrical parameters of device are obtained [12]. Besides, it affects the delayed degradation of perovskite [8]. Other common HTMs are poly(triarylamine), poly(3-hexylthiophene) [13] or carbazole [14]. Interesting group of organic materials that can be found as hole transporting materials are azomethines. They are compounds with HC═N— groups known also as Schiff bases. Due to their donor properties it is possible to apply them in organic photovoltaics [15].

Among inorganic HTMs, Cu based inorganic semiconductors, quantum dots and Kesterites can be distinguished [11,16–18].

Despite all, the high performance and cheap HTM, and effective perovskite protective obstacle are still required. For this reason, the main goal of this work was to test two polyazomethines as HTMs and as a protective barrier in perovskite solar cells. Polyazomethines (PAZ) have been investigated over the past 30 years mainly as thermostable, biological, and liquid crystalline (LC) compounds [19,20]. However, in the last 16 years PAZs are also investigated as a donor component of an active layer in polymer solar cells [21–37]. The first article about polymer solar cells with PAZ was published by Sharma et al. in 1996 [23]. The authors studied the photovoltaic properties of poly(phenyl azomethine furane) (PPAF) in a monolayer device with a Ag/PPAF/ITO architecture and received a photoconversion efficiency (PCE) value of approximately 0.019%. The highest value of PCE, i.e., 0.52%, was obtained by our group for the polymer solar cell with the active layer based on $PC_{71}BM$ and polyazomethine with three thiophene rings per unit [25] and for polyazomethine with triphenylamine and p-terphenyl moieties (PCE = 0.56%) [27].

In this work two various HTM layers in perovskite solar cells are analyzed varying the chemical structure of polymer in perovskite devices. Taking into account the thermal and air stability of polyazomethines, we proposed two PAZs: one with three thiophene rings and 3,3′-dimethoxybenzidine moieties (S9) and second one with three thiophene rings and fluorene moieties (S7) investigated as HTMs in perovskite solar cells. Independently, due to the high stability, PAZs were examined as a protection barrier to avoid degradation. Therefore, the aim of this work was to PAZs bifunctionality presentation showing possibility for application in

Table 1
The FTIR and TGA data of polymers.

Code	Properties
S7	Yield 88%. FTIR, ν [cm^{-1}]: 3063 (aromatic C–H stretching), 1659 (C═O stretching from residue CHO groups), 1610 (C═N imine stretching), 1590-1442 (stretching in the aromatic ring), 788 (bending C—H out of plane). TGA, $T_{5\%}$ $T_{10\%}$ and $T_{25\%}$ weight loss at 406 °C, 439 °C and 567 °C, respectively. Char yield at 61% (Residual weight when heated to 800 °C).
S9	Yield 40%. FTIR, ν [cm^{-1}]: 3063 (aromatic C—H stretching), 2932 (aliphatic C—H stretching), 2830 (C—H stretching from residue CHO groups), 1660 (C═O stretching from residue CHO groups), 1607 (C═N imine stretching), 1593-1440 (stretching in the aromatic ring), 1236 (aromatic C—O stretching), 1132 (C—C stretching between aromatic rings), 1030 (aliphatic C—O stretching), 792 (bending C—H out of plane). TGA, $T_{5\%}$, $T_{10\%}$ and $T_{25\%}$ weight loss at 377 °C, 390 °C and 493 °C, respectively. Char yield at 58% (Residual weight when heated to 800 °C).

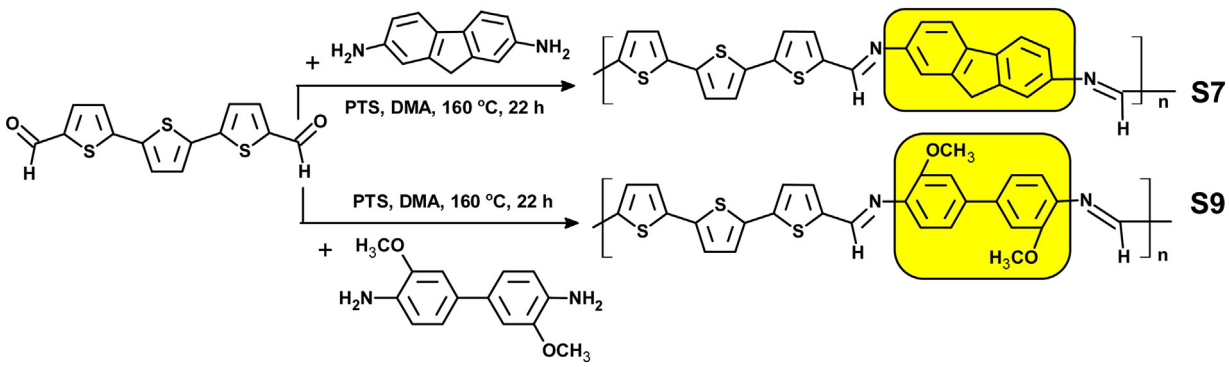

Fig. 3. Synthetic route of polyazomethines S7 and S9 with thiophene rings.

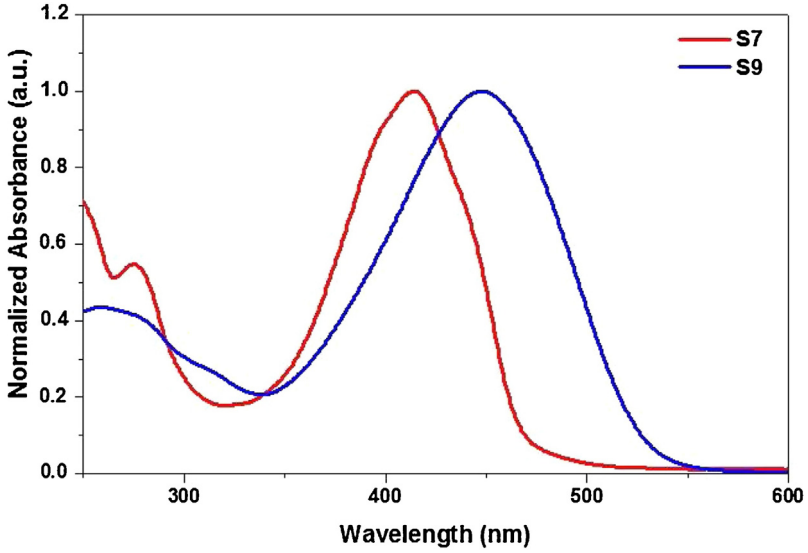

Fig. 4. UV–vis spectra of S7 and S9 in chloroform solution.

the inexpensive photovoltaics. Electrical parameters were investigated under an illumination of 100 mW/cm^2 with an AM1.5G. To the best of our knowledge, this is the first time that perovskite solar cells with S7 and S9 polyazomethines as HTM are analysed.

2. Experimental

2.1. Materials

2,2':5',2"-Terthiophene-5,5"-dicarboxaldehyde, 3,3′-dimethoxybenzidine, 2,7-diaminofluorene, *N,N*-dimethylacetamide (DMA), chloroform, lead iodide (PbI_2) (purity 99%), anhydrous *N,N*-dimethylformamide (DMF) (purity 99.8%) were purchased from Sigma-Aldrich and used as received. Methanol, ethanol (purity 96%) and acetone were purchased from POCH and used as received. Hydrochloric acid (36–38%) was purchased from CHEMPUR.

Titanium (IV) ethoxide ($C_8H_{24}O_4Ti$) was purchased from Merck. FTO, MAI powder and TiO_2 paste T600/sp were purchased from Solaronix.

2.1.1. Synthesis of S9 and S7

The polymers were obtained using an one-step high temperature condensation technique with anhydrous $CaSO_4$ as the water trap. A single-neck flask with a magnetic stir bar was charged with dialdehyde (1 mmol), diamine (1 mmol), *p*-toluenesulfonic acid (PTS) and 10 mL of DMA. The reaction mixture was allowed to stir for 22 h at 160 °C in an oil bath. The polymer solution was precipitated in methanol, and the polymer was collected by filtration. The solid was washed with hot methanol and hot acetone. The final polymer was dried overnight at 80 °C. Preparation of polymer S9 was described in details inRRef. [25].

Both polymers were used in the perovskite solar cells as HTM. The 36 mg of each polymer were dissolved in 1 ml of chloroform and deposited on perovskite by using Headway Research Inc. spin coater, 2000 rpm for 30 s.

2.1.2. Preparation of blocking b-TiO_2 layer

TiO_2 blocking layer was prepared by using sol-gel method. The sol solution was a mixture of 1.14 g of tetraethyl ortotitanate, 10 ml of ethanol and 0.2 ml of hydrochloric acid. The sol was deposited on a glass with FTO by a spin coater (3500 rpm, 15 s.). Subsequently, the substrates were dried at 200 °C for 10 min and then annealed at 500 °C for 1 h to obtain anatase crystal phase.

2.1.3. Preparation of mesoporous scaffold

The TiO_2 paste T600/sp was screen printed on a glass with b-TiO_2 to create a mesoporous scaffold. The annealing process was preceded by drying at 200 °C for 10 min, and conducted at 500 °C during 1 h.

2.1.4. Preparation of perovskite layer

To prepare the perovskite layer, a two-step deposition method was used. In the first step PbI_2 and MAI solutions were prepared

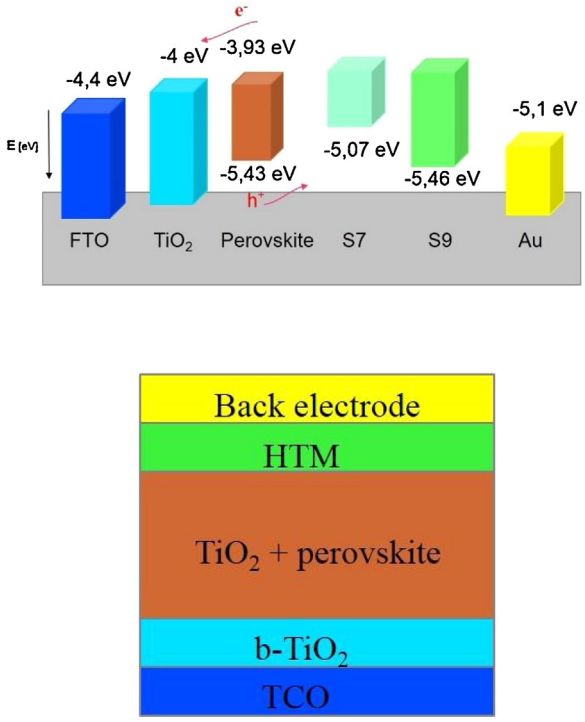

Fig. 5. Energy band diagram for perovskite solar cell on a scaffold structure with S7 and S9 as HTM, and schematic cross section of the device architecture.

as following: 1.39 g PbI_2 was dissolved in 3 ml of anhydrous *N,N*-dimethylformamide, DMF at 70 °C for 30 min with stirring and 0.1 g of MAI powder was dissolved with 10 ml isopropanol (IPA). Then, lead iodide layer was put down on a scaffold by spin coating 1500 r.p.m for 30 s. and dried at 70 °C for 3 min and at 90 °C for 5 min. Subsequently substrates were dipped in MAI solution for 5 min rinsed in IPA and dried at 90 °C for 30 min.

2.2. Characterisation

The FTIR characterization of the obtained polymers was carried out by Nicolet 5700 (ThermoElectron). UV–vis spectra were recorded in a chloroform solution by Jasco V670 spectrophotometer. Thermogravimetric analyses (TGA) were performed on a Mettler-Toledo AG apparatus at a heating rate of 10 °C/min under nitrogen. Conductivity (σ) of S7 and S9 layers was measured for ITO/S7 (or S9)/Al structure by two-probe method using Keithley 2400 source meter at a temperature of 25 °C for 100, 200 and 500 mV bias. Temperature was controlled by a thermometer. An aluminum electrode (thickness about 80 nm) was deposited by thermal evaporation in a vacuum of approximately 6.67×10^{-2} Pa. The thickness of the S7 and S9 layer was determined using the AFM technique (with a sharp copper blade) by measuring the height of the edge.

The AFM measurements were performed using intermittent contact mode in air and room temperature (25 °C, RH = 35%). The Innova instrument from Bruker was used. Typical probes were utilized to perform the measurements (about 40 N/m and <10 nm tip radius). Acquired data was analyzed using SPIP software from Image Metrology.

The PerkinElmer UV/VIS/NIR Spectrometer Lambda 950S was used to perform optical measurements of perovskite. The Philips X'Pert X-ray diffractometer PW 1710 with Co Kα radiation was applied to confirm that obtained material is $CH_3NH_3PbI_3$.

Electrical parameters of solar cells with different HTM layers were measured by solar cells' I–V curve tracer with solar radiation simulator PET PHOTO EMISSION TECH., INC. at STC conditions (cell temperature of 25 °C, irradiance of 1000 W/m^2, AM1.5). The cell area was equal to 0.25 cm^2. Gold electrode was deposited by thermal evaporation in vacuum of about 5×10^{-4} Pa. Constructed devices were investigated without any encapsulation.

3. Results and discussion

3.1. Perovskite characterisation

Obtained perovskite samples were examined by UV–vis and XRD experiments to confirm their structure. The optical measurements were done using transmission mode, and they led to determine the band gap energy (Eg) of $CH_3NH_3PbI_3$ by using Tauc plot (Fig. 1) and formula for direct band gap [7].

The value of the perovskite band gap was estimated at 1.57 eV. This is in agreement with values reported recently in the literature [1]. Therefore, it can be deduced that synthesized perovskite possesses adequate optical properties and the solar cell will be operating within the 400–800 nm spectral range.

In order to obtain further confirmation of the phase composition of synthesized perovskite XRD measurements were performed. As can be seen, from the diffractogram (see Fig. 2) of perovskite powder, the measured peaks are correlated with values from data base. Diffractogram confirms that beta-methylamminium lead triiodide was obtained similarly to other literature report [38] and it has a tetragonal structure.

3.2. Polyazomethines' characterisation

Both polyazomethines were prepared using a simple, one-step, high-temperature, condensation procedure with the catalyst in solution. The synthesis of both polyazomethines (S7 and S9) is outlined in Fig. 3.

FTIR and TGA data of polymers S7 and S9 are presented in Table 1.

The presence of imine groups was confirmed by FTIR spectroscopy, and in each case, the band characteristics of the –HC=N– stretching deformations at 1607 cm^{-1} (for S9) and 1610 cm^{1} (for S7) was observed. The band characteristics of the carbonyl end group was also observed at approximately 1660 cm^{-1}.

The thermal properties of both polyazomethines were characterized by a thermogravimetric analysis (TGA) performed in a nitrogen atmosphere at a heating rate of 10 °C/min to 800 °C (Table 1). The TGA experiment of S7 and S9 indicates one main reaction stage. The thermal properties of investigated polymers depended on the structure of polyazomethines, in this case on the sub-unit of the polymer backbone. The initial decomposition based on a 5% weight loss and the temperature at which 10% weight loss occurred (which is usually considered the criterion for assessing the thermal stability) lay within the range of 377–406 °C and 390–439 °C, respectively (see Table 1). Our study showed that polymer S7 started to decompose at about 29 °C higher temperature (406 °C) than S9 polyazomethine (377 °C). Moreover, taking into account the amount of carbonized residue, not significant differences between both polymers were found. The char yield percent at 800 °C was found at 61% for S7 and 58% for S9. The high thermal stability of the polymers prevents deformation of their morphology and it is important for polymeric photovoltaic device applications. Aromatic polyazomethines are an attractive class of high performance polymers, due to their high thermal stability [19].

Currently, a lot of efforts have been made towards improving thermal stability of perovskite solar cell. Taking into consideration application of perovskite solar cells outdoors, one very important issue is analysing an effect of thermal stability of organic layers on

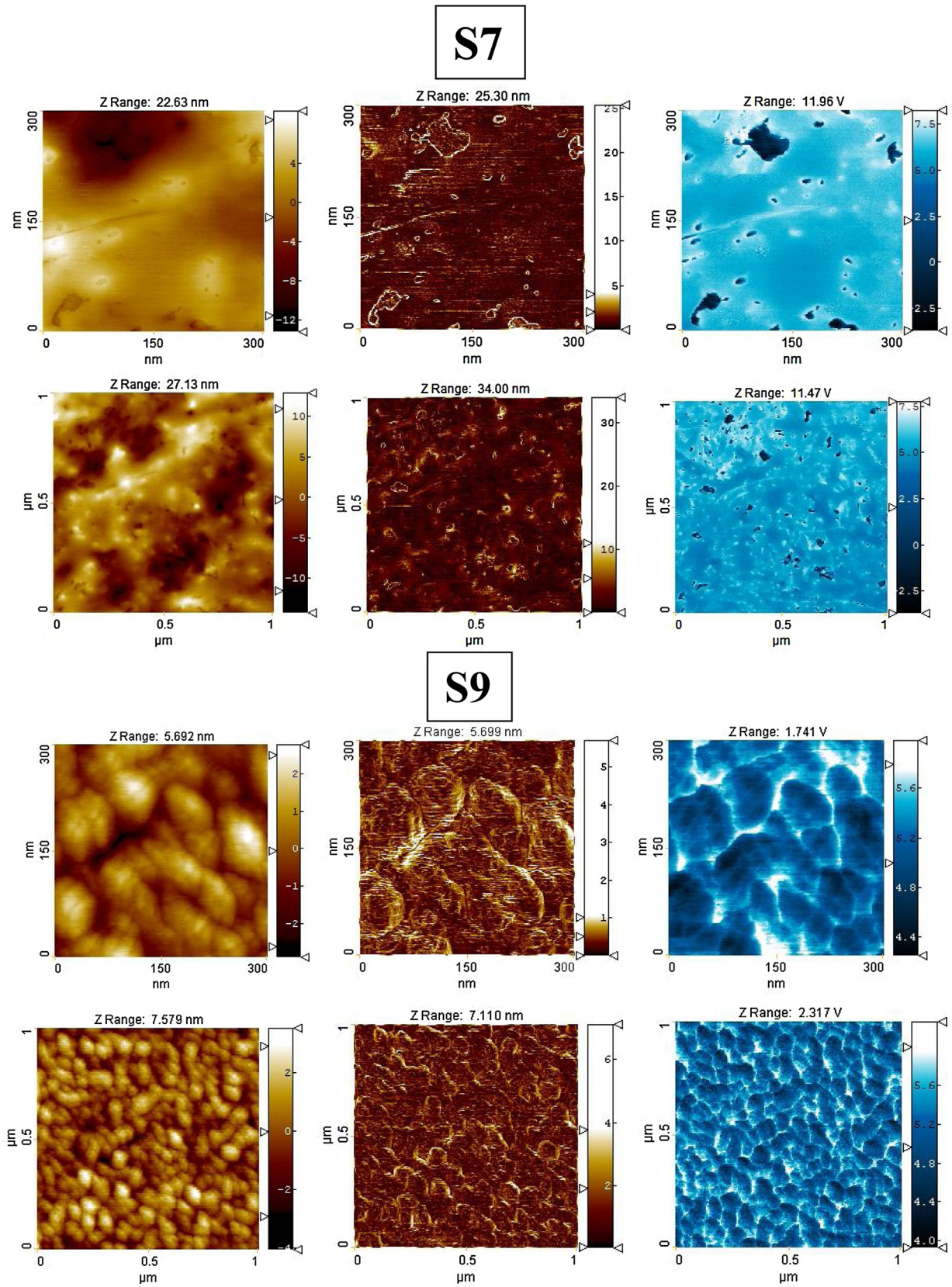

Fig. 6. AFM images (topography), Sobel transform and the Phase Imaging of S7 and S9 polyazomethines.

the properties of the devices. According literature [19], investigated in this work, polyazomethines exhibited good thermal properties compared with other polyazomethines.

The conductivity (σ) of S9 and S7 was approximately of 2.6×10^{-10} S/cm and 2.7×10^{-8} S/cm, respectively. As the voltage increased from 100 to 500 mV, a small increase in the conduc-

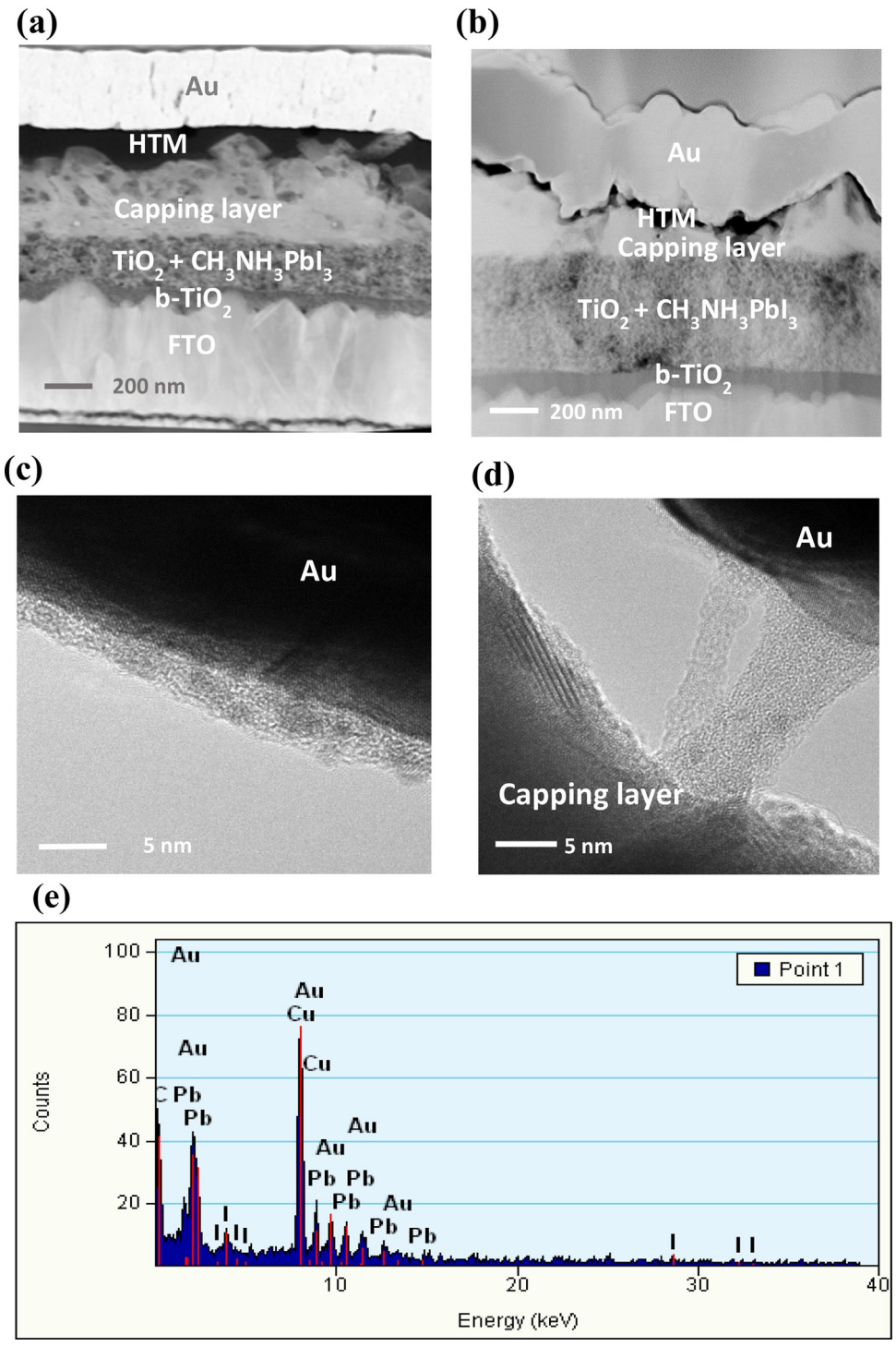

Fig. 7. (a) The cross sectional STEM image of the perovskite solar cell with typical HTM (Spiro-OMeTAD), (b) The cross sectional STEM image of the perovskite solar cell with tested polymer (S9), (c) HRTEM micrograph of the gold surface covered by thin amorphous layer, (d) HRTEM micrograph of the polymer fiber located between perovskite capping layer and back electrode (Au), (d) EDX analysis result of the amorphous fiber.

tivity of the both polymers was observed. For example, for S9 the conductivity at 500 mV was 4.3×10^{-10} S/cm, while for S7 $\sigma = 3.1 \times 10^{-8}$ S/cm was found. Thickness of S9 was 11.9 nm, while for S7 6.4 nm, as detected by the AFM method.

The introduction of dimethoxybenzidine in S9 polyazomethine resulted in a bathochromic shift of the absorption band maximum compared to S7 (from 415 nm to 446 nm). This absorption peak, which was observed as a well-defined band in the UV–vis spectra of the polyazomethines, is due to the π-π^* transition in the imine group (see Fig. 4).

The electrochemical properties of the studied polymers were investigated in CH_2Cl_2 using cyclic voltammetry (CV). For S9 details of CV experiments can be found in our previous paper [25]. Briefly, HOMO and LUMO levels of S9 polyazomethine were found at −5.46 eV and −2.79 eV, while of S7 polymer at −5.07 eV and −2.19 eV, respectively. Energy gap (Eg) of S9 was detected at 2.67 eV, while for S7 Eg = 2.88 eV. Energy level diagram of S9 and S7

Table 2
The surface parameters of both polyazomethines investigated by AFM.

Code	Surface statistics[a]				
	R_a [nm]	R_{ms} [nm]	Skewness	Kurtosis	Surface Area Ratio [%]
S7 (300 nm × 300 nm)	2.72	3.61	−0.95	3.71	10.42
S7 (1 nm × 1 nm)	3.21	4.04	−0.17	2.88	2.24
S9 (300 nm × 300 nm)	0.65	0.82	0.03	3.17	0.53
2 S9 (1 nm × 1 nm)	0.77	0.96	0.02	2.90	0.68

R_a: value of the height irregularities (arithmetic average of absolute values). Exponent (power) within the data variance sum for the RMS is q = 1. The Roughness Average, is defined as: $R_a = \frac{1}{MN}\sum_{k=0}^{M-1}\sum_{l=0}^{N-1}|z(x_k, y_l)|$.

R_{ms}: value of the height irregularities (Root Mean Squared). Exponent (power) within the data variance sum for the RMS is q = 2. The Root Mean Square (RMS) parameter R_{ms} (S_q), is defined as: $R_{ms} = \sqrt{\frac{1}{MN}\sum_{k=0}^{M-1}\sum_{l=0}^{N-1}[z(x_k, y_l)]^2}$, where: M and N are the total number of pixels in the analyzed scan, k and l are coordinates of a given pixel, z (x_k, y_l) is the height of the surface at a given coordinate.

[a] values calculated for scanning field 300 nm × 300 nm and 1 nm × 1 nm.

Table 3
Electrical parameters of constructed perovskite solar cells.

HTM	V_{oc} [mV]	I_{sc} [mA]	FF	PCE [%]	R_{s0} [Ω]	R_{sh0} [kΩ]
S9	830	4.4	0.41	6.1	77.1	1.02
S7	832	4.8	0.43	6.9	89.8	0.71
w/o	841	5.8	0.50	9.6	32.2	0.77

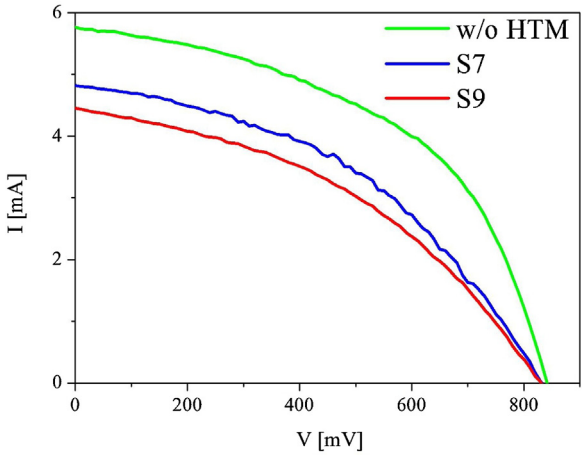

Fig. 8. I–V characteristics of perovskite solar cells with various HTM, under AM 1.5 G-simulated solar illumination (100 mW/cm^2), cell area 0.25 cm^2.

based on CV experiment is presented in Fig. 5 along with architecture of constructed perovskite devices.

The morphology of both polyazomethines was studied using AFM. Fig. 6 shows a typical, planar view of the topography, and the Sobel transform, which we used to provide a better view of fine structures and features. In addition, the Phase Images were presented, which show maps of viscoelastic forces, useful for imaging inhomogeneous materials.

Investigated samples differ significantly in terms of morphological properties. S7 sample reveals complex structure of the surface, which is relatively smooth and wavy, however, the presence of the grains embedded in the surface, can be noted. The size of the grains is difficult to determine, due to the fact, that they seem to be covered by outer layer. However, their approximate diameter is in the range of 10–30 nm. The distribution of the grains is non-homogenous, the amount is few dozen per one square micrometer. Moreover, the holes in outer layer can be noted during the analysis of both: topographical and phase imaging data. In addition, the changes of the viscoelastic properties of the surface visible as the changes of the phase imaging data, in particular in areas with reduced density of grains, seem to vary. Concerning the mechanical response in the area of the discontinuities of the outer layer, one can argue, that in the vicinity of the grains, the outer layer is thicker, than in other areas.

On the other hand, the surface of S9 sample is covered with round and elliptical grains, approx. 50–100 nm in diameter. No significant mechanical non-homogeneities can be described basing on phase data. The only visible features are related to the space between the grains, where the tip-sample interaction varies due to changes of the active contact surface, therefore, one should consider it as the artifacts.

It should be underlined, that the height of the structures in case of S7 sample is bigger than in S9 sample, therefore all the roughness parameters reached significantly higher values. The dominant objects for S7 sample are rare holes, therefore skewness is below 0. On the other hand, grainy and homogenous structure of S9 sample is correlated with skewness value slightly above 0.

The roughness parameters such as (R_a, R_{ms}), skewness (the unbalance of height distribution maximum) and kurtosis (the peak's width on height distribution) for the investigated surfaces are presented in Table 2.

3.3. Photovoltaic experiments

The perovskite solar cells were fabricated using the described above perovskite absorber in the standard architecture shown in Fig. 5. The top electrode was a transparent conductive oxide (fluorine doped tin oxide, FTO) while back electrode was made from high work function metal (Au). Perovskite solar cells using S7 and S9 polyazomethines as an HTM were fabricated and their photovoltaic parameters were compared with device without HTM layer. The cross-sectional STEM image (see Fig. 7a) has shown the perovskite solar cell with typical HTM (Spiro-OMeTAD). As can be seen, the perovskite partially crystallized within the porous titanium dioxide layer and also formed thick capping layer which was crystallized on to the porous TiO_2. The presence of capping layer should be beneficial because it helps to avoid direct contact between HTM and electron conducting TiO_2 and, hence decrease the recombina-

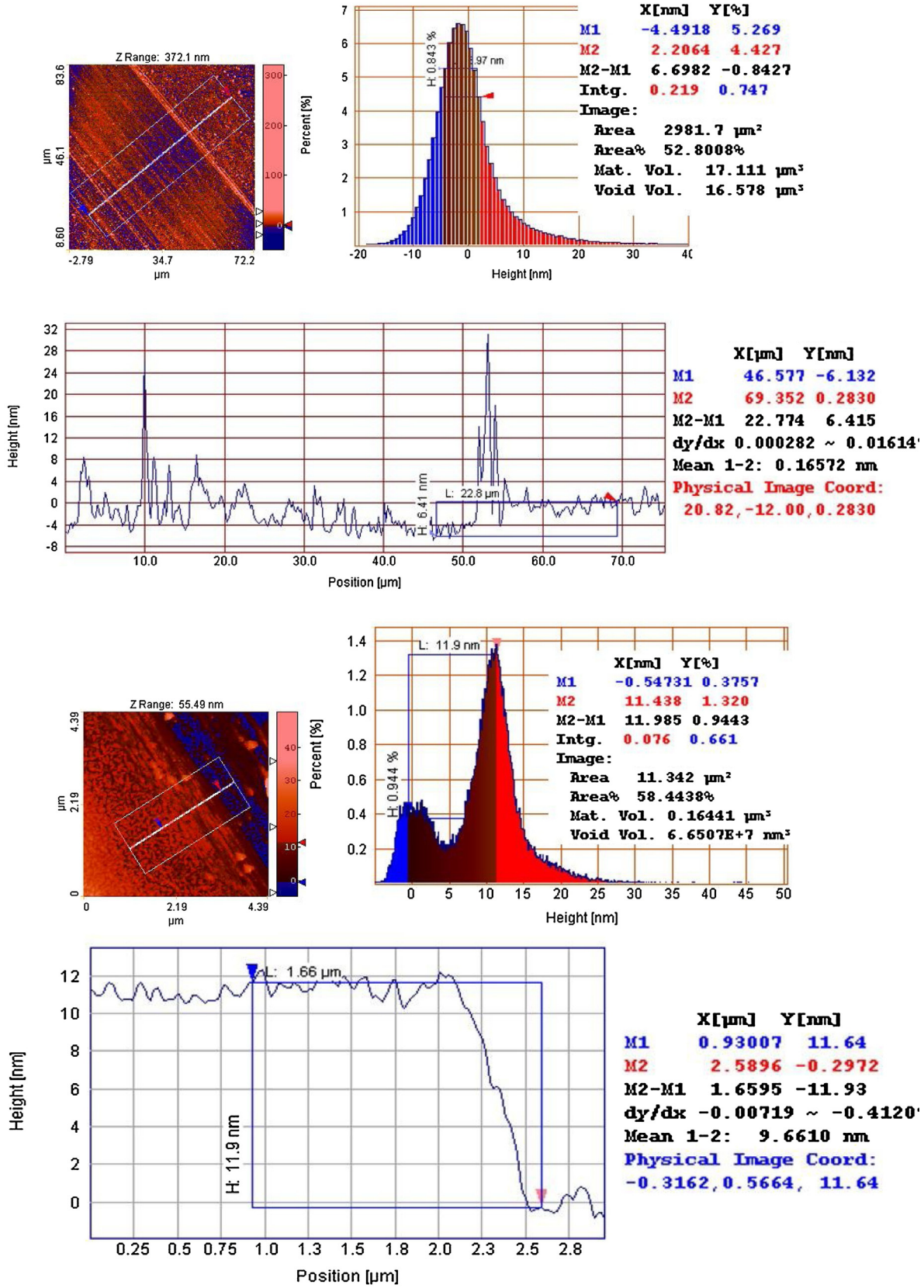

Fig. 9. Thickness of S7 (top) and S9 (bottom) polyazomethines measured using AFM.

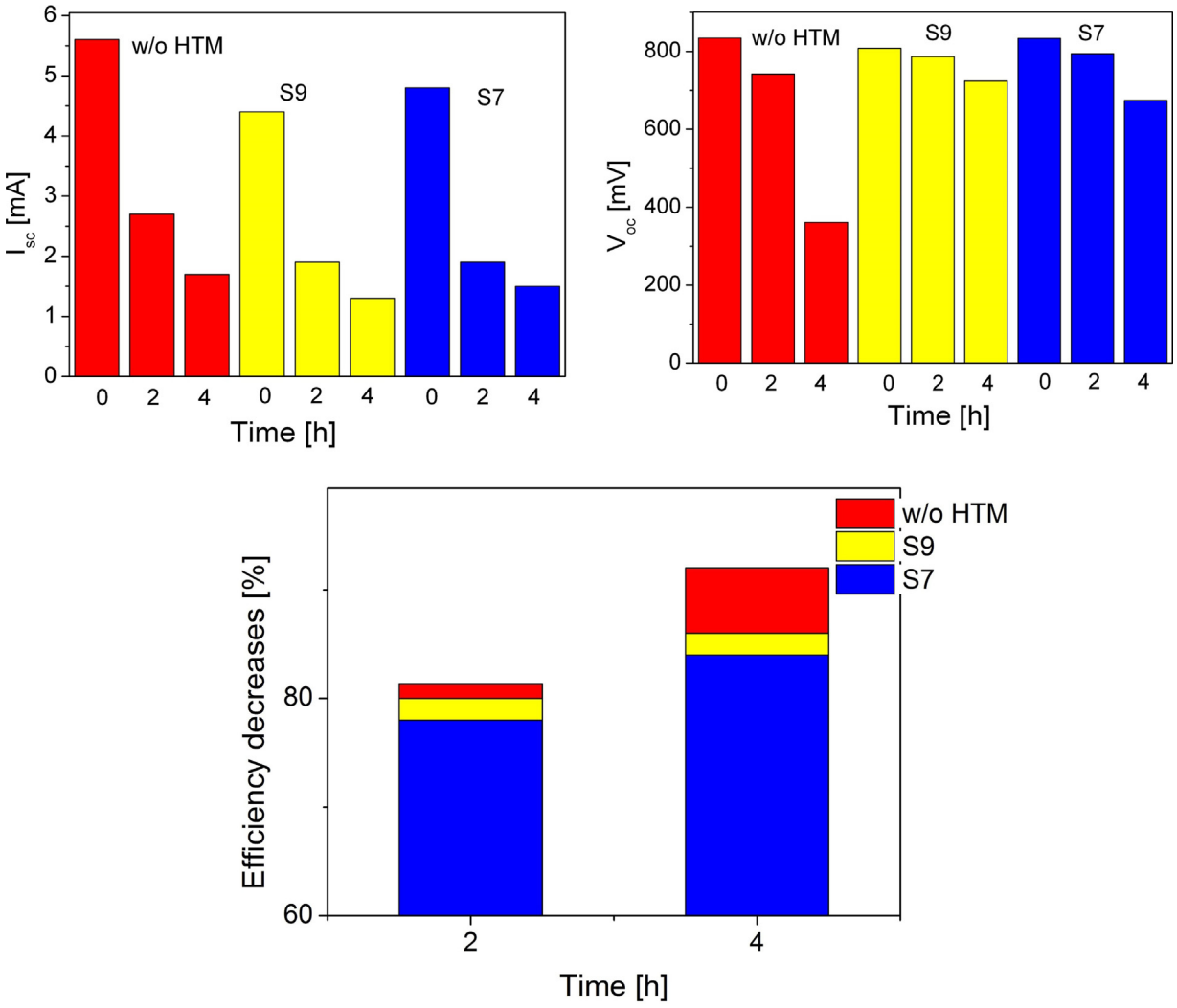

Fig. 10. Diagrams of decrease of Voc, Isc and efficiency of investigated perovskite solar cells in time (0–4 h).

tion. However, it introduced the considerable surface roughness that should be well covered by HTM material. In this exact image, the Spiro-OMeTAD layer appeared in the right morphology, namely totally, separating the perovskite from gold electrode.

While Fig. 7(b) has shown a perovskite solar cell with polymer S9 and in this case HTM creates very thin and not uniformly distributed coating. Therefore, full layers separation is not provided and the places where gold touches perovskite are observed. The characteristic, black outline at the bottom of the back electrode layer, is caused by the polymer presence on the gold surface, which is confirmed by the HRTEM image [Fig. 7(c)], where amorphous coating on gold is observed.

It is worth to pointing out that the roughness of the bottom of the gold and perovskite capping layer, do not fit together what would be observed if the polymer was not there. The Fig. 7(d) presents the very thin amorphous fiber localized between perovskite capping layer and gold electrode. The EDX analysis has confirmed strong increase of the carbon signal for this fiber what indicates that it is an applied polymer Fig. 7(e).

Electrical parameters of solar cells were measured by solar cells I–V curve tracer. The contact to both electrode was gained by using homemade handle. The open circuit voltage values are similar for all devices, while, short circuit current is much lower for perovskite solar cells with polymers S7 and S9 (Table 3). Such behaviour is a consequence of high value of R_{s0}. The causes of high series resistance are a problems with carriers movement in solar cells or significant contact resistance. In this case, higher R_{s0} for solar cells with polymers S7 and S9 seems to be a result of difficulties with carriers movement in solar cells. Moreover, low shunt resistance, which reduces the amount of current flowing through the solar cell junction as a result of high leakage, can either has an influence on Isc. Both resistances have also significant impact on fill factor which is an important parameter carrying an information about curve deviation from perfect rectangle. Low FF means high deviation what is clearly watchable in Fig. 8.

The best performance, among two investigated polyazomethines, was obtained for device with the following architectures FTO/TiO_2/TiO_2 + perovskite/S7/Au. A PCE of 6.9% with open circuit voltage V_{oc} = 832 mV, short circuit current I_{sc} = 4.8 mA, and fill factor FF = 0.43 were achieved. The PV parameters for all devices, investigated in this work, are listed in Table 3.

The dynamic series resistance (R_{s0}) and dynamic shunt resistance (R_{sh0}) are given by Eqs. (1) and (2):

$$R_{s0} = -(\partial G\,V/\partial Gi)_{V=Voc} \quad (1)$$

$$R_{sh0} = -(\partial G\,V/\partial Gi)_{i=Isc} \quad (2)$$

where i and V terminal current and voltage, respectively.

The I–V (current-voltage) characteristics of the perovskite solar cells based on polyazomethines are shown in Fig. 8. Green line presents perovskite solar cell without any HTM, blue is a solar

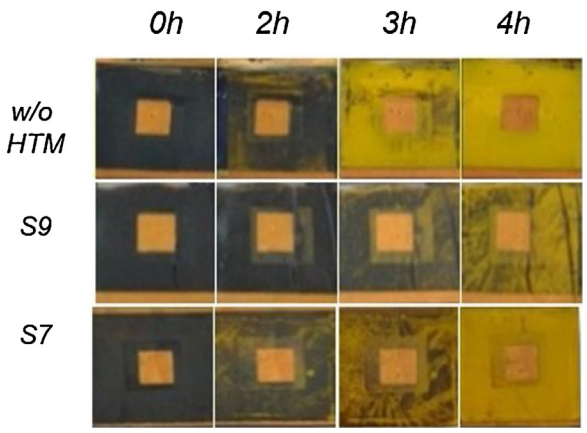

Fig. 11. Picture of degradation of perovskite solar cells without and with polyazomethines in time.

device with polymer S7 and red with polymer S9. The shape of curves is an effect of high value of series resistance and low shunt resistance.

No significant changes in the PV parameters for perovskite devices based on S7 or S9 polyazomethines were observed. Some differences were found in the series (R_{s0}) and shunt (R_{sh0}) dynamic resistance of the devices with polyazomethines. High value of series resistance 77.1 Ω for device with S7 polyazomethine and 89.8 Ω for solar cell with S9 demonstrates that resistivity of these layers is high which can be explained by low carrier mobility or low acceptor concentration. Moreover, both investigated polyazomethines are not well soluble in chloroform and for this reason the obtained layer is very thin and not uniform (from 0 to even 170 nm in a final perovskite solar cell structure).

Thickness of S7 and S9 polyazomethines was also measured by AFM experiment (see Fig. 6). Thickness of S7 polyazomethine was of about 6.4 nm, while for S9 was 11.9 nm. In order to measure film thickness, the surface was scratched with a copper wire, as the step edge makes the topographical analysis possible. Two methods: surface height distribution and edge profile analysis were applied with good agreement (Fig. 9). It should be emphasized, that the profile lines were acquired as the average value of the set of at least 50 neighbourhood single profiles (indicated by white squares).

Unfortunately, electrical parameters of perovskites devices with polymers S7 and S9 as HTM were worse than for perovskite solar cell without HTM. However, it should be stressed that obtained value of PCE of perovskite solar cells with polyazomethines are the highest to best of our knowledge taking into consideration polyazomethines used in photovoltaics. In our previous work [25] polymer S9 was applied as a donor component of the active layer in bulk heterojunction (BHJ) polymer solar cells with the ITO/PEDOT:PSS/S9:$PC_{71}BM$ (1:2)/Al architecture and maximum value of PCE at 0.52% under simulated 100 mW/cm^2 AM 1.5G irradiation was obtained.

Except holes transport, HTM should also protect the perovskite layer [9]. For this reason in the next step of our work, the polyazomethines protective impact on perovskite devices was checked. In Fig. 10 we graphically presented how not encapsulated perovskite solar cells without and with polyazomethine HTM, were degraded in time (0–4 h) upon full sun light conditions.

After 4 h, reduction of I_{sc} was similar for all samples, approximately 70% of primal value, from 5.8 mA to 1.7 mA for PSC without HTM, from 4.8 mA to 1.5 mA for device with S7 and from 4.4 mA to 1.3 mA for solar cell with polymer S9. Drop of open circuit voltage (V_{oc}) for device without HTM was high, from 844 mV to 742 mV after 2 h and to 361 mV after 4 h of ageing. While solar cells with polymers S7 and S9 are characterised by lower V_{oc} decreased. For PSC with S7 as HTM, the Voc has fallen from 832 mV to 794 mV and to 674 mV after respectively 2 and 4 h of sun exposition and from 830 mV to 786 mV and to 724 mV for PSC with polymer S9. The efficiency decreases was about 8% and 6% lower for solar cells with polymer S7 and S9 than for devices without any HTM. This demonstrates protective properties of polymers S7 and S9 on perovskite, what has been clearly shown in Fig. 11. The results are very promising and they indicate that regardless of weak solubility of S9 and S7 in chloroform, the polymers layers were present on perovskite. Finally, we can conclude slower degradation of PSCs with polyazomethine HTM in respect to devices without HTM. To obtain better electrical parameters of perovskite solar cells, carrier mobility of S7 and S9 improvement is necessary and thickness optimization of HTM layer has to be done.

4. Conclusions

In this work two polyazomethines with three thiophene rings called S7 and S9 were examined as potential hole transporting materials in perovskite solar cells. We found, that both polymers protect perovskite which is confirmed by ageing test where V_{oc} did not decrease significantly for solar cells with HTM in contrast to solar cell without hole conductor where V_{oc} decrease was substantial. The best performance among two investigated in this work polyazomethines was obtained for a device with the following architectures FTO/TiO_2/TiO_2 + perovskite/S7/Au, where polyazomethine with fluorene moieties was used as HTM. Under these conditions, a PCE of 6.9% with open circuit voltage V_{oc} = 0.832 V, short circuit current I_{sc} = 4.8 mA, and fill factor FF = 0.43 were achieved.

Finally, we would like to stress that our idea to apply cheap, air- and thermally stable polyazomethines as HTM is, in our point of view, very promising compare with the results presented in Ref. [39], where such commercial polymers as P3HT, PCDTBT and PCPDTBT were applied as HTM. PCE value of these polymers in perovskite solar cells was of 6.7%, 4.2% and 5.3%, respectively.

We believe that our results will be an inspiration for scientists work in photovoltaics. Next researches have to be done to improve electrical parameters of solar cells with S9 and S7 as HTM and solubility of polyazomethines.

Acknowledgements

The authors gratefully acknowledge the financial support from Polish National Science Centre under the grant No. DEC-2012/05/B/ST8/00087 and the National Centre for Research and Development under the 2012–2015 project No. PBS1/A5/27/2012.

Authors thank Mr K. Parafiniuk for synthesis and IR analysis of the polymers, Mr L. Gorecki for TGA experiment, Dr. A. Goral for XRD measurement and Prof. L. Major for STEM analysis.

References

[1] G.E. Eperon, S.D. Stranks, C. Menelaou, M.B. Johnston, L.M. Herz, H.J. Snaith, Formamidinium lead trihalide: a broadly tunable perovskite for efficient planar heterojunction solar cells, Energ Environ. Sci. 7 (2014) 982.
[2] L. Zheng, D. Zhang, Y. Ma, Z. Lu, Z. Chen, S. Wang, L. Xiao, Q. Gonga, Morphology control of the perovskite films for efficient solar cells, Dalton Trans. 44 (2015) 10582–10593.
[3] A. Hagfeldtt, M. Gratzel, Light-induced redox reactions in nanocrystalline systems contents, Chem. Rev. 95 (1995) 49–68.
[4] W. Nie, H. Tsai, R. Asadpour, J.Ch. Blancon, A.J. Neukirch, G. Gupta, J.J. Crochet, M. Chhowalla, S. Tretiak, M.A. Alam, H.L. Wang, A.D. Mohite, High-efficiency solution-processed perovskite solar cells with millimeter-scale grains, Science 347 (2015) 522–525.
[5] J.H. Heo, H.J. Han, D. Kim, T.A. Ahn, S.H. Im, Hysteresis-less inverted CH3NH3PbI3 plan perovskite hybrid solar cells with 18.1% power conversion efficiency, Energy Environ. Sci. 8 (2015) 1602.

[6] J.A. Christians, P.A. Herrera, P.V. Kamat, Transformation of the excited state and photovoltaic efficiency of CH3NH3PbI3 perovskite upon controlled exposure to humidified air, J. Am. Chem. Soc. 137 (2015) 1530–1538.
[7] G.E. Eperon, V.M. Burlakov, A. Goriely, H.J. Snaith, Neutral color semitransparent microstructured perovskite solar cells, ACS Nano 8 (2014) 591–598.
[8] J. Liu, S. Pathak, T. Stergiopoulos, T. Leijtens, K. Wojciechowski, S. Schuman, N. Kausch-Busies, H.J. Snaith, Employing PEDOT as the p-type charge collection layer in regular organic-inorganic perovskite solar cells, J. Phys. Chem Lett. 6 (2016) 1666–1673.
[9] A. Gheno, S. Vedraine, B. Ratier, J. Bouclé, π-Conjugated materials as the hole-transporting layer in perovskite solar cells, Metals 6 (2016) 21.
[10] Ch Huang, W. Fu, Ch.-Z. Li, Z. Zhang, W. Qiu, M. Shi, P. Heremans, A.K.-Y. Jen, H. Chen, Dopant-free hole-transporting material with a C3 h symmetrical truxene core for highly efficient perovskite solar cells, J. Am. Chem. Soc. 138 (2016) 2528–2531.
[11] M. Lv, J. Zhu, Y. Huang, Y. Li, Z. Shao, Y. Xu, S. Dai, Colloidal CuInS2 quantum dots as inorganic hole-transporting material in perovskite solar cells, ACS Appl. Mater. Interfaces 7 (2015) 17482–17488.
[12] D.H. Sin, H. Ko, S.B. Jo, M. Kim, G.Y. Bae, K. Cho, Decoupling charge transfer and transport at polymeric hole transport layer in perovskite solar cells, ACS Appl. Mater. Interfaces 8 (2016) 6546–6553.
[13] Ch. Tao, S. Neutzner, L. Colella, 17.6% stabilized efficiency in low-temperature processed panar perovskite solar cells, Energy Environ. Sci. 8 (2015) 2365–2370.
[14] S.D. Sung, M.S. Kang, I.T. Choi, H.M. Kim, H. Kim, M. Hong, H.K. Kim, W.I. Lee, 14.8% perovskite solar cells employing carbazole derivatives as hole transporting materials, Chem. Commun. 50 (2014) 14161–14163.
[15] M.L. Petrus, T. Bein, T.J. Dingeman, P. Docampo, A low cost azomethine-based hole transporting material for perovskite photovoltaics, J. Mater. Chem. A 3 (2015) 12159–12162.
[16] Q. Wu, C. Xue, Y. Li, P. Zhou, W. Liu, J. Zhu, S. Dai, Ch. Zhu, S. Yang, Kesterite Cu2ZnSnS4 as a low-cost inorganic hole-transporting material for high-efficiency perovskite solar cells, ACS Appl. Mater. Interfaces 7 (2015) 28466–28473.
[17] X. Liu, Y. Feng, H. Cui, F. Liu, X. Hao, G. Conibeer, D.B. Mitzi, M. Green, The current status and future prospects of kesterite solar cells: a brief review, Prog. Photovoltaics 24 (2016) 879–898.
[18] Q. Wu, C. Xue, Y. Li, P. Zhou, W. Liu, J. Zhu, S. Dai, C. Zhu, S. Yang, Kesterite Cu2ZnSnS4 as a low-cost inorganic hole-transporting material for high-efficiency perovskite solar cells, ACS Appl. Mater. Interfaces 7 (2015) 28466–28473.
[19] A. Iwan, D. Sek, Processible polyazomethines and polyketanils: from aerospace to light emitting diodes and other advanced applications, Progr. Polym. Sci. 33 (2008) 289–345.
[20] A. Iwan, D. Sek, Polymers with triphenylamine units: photonic and electroactive materials, Prog. Polym. Sci. 36 (2011) 1277–1325.
[21] A.W. Jeevadason, K.K. Murugavel, M.A. Neelakantan, Review on Schiff bases and their metal complexes as organic photovoltaic materials, Renew. Sustain. Energy Rev. 36 (2014) 220–227.
[22] M. Palewicz, A. Iwan, M. Sibiński, A. Sikora, B. Mazurek, Organic photovoltaic devices based on polyazomethine and fullerene, Energy Procedia 3 (2011) 84–91.
[23] G.D. Sharma, S.G. Sandogaker, M.S. Roy, Electrical and photoelectrical properties of poly(phenyl azomethine furane) thin films devices, Thin Solid Films 278 (1996) 129–134.
[24] A. Iwan, M. Palewicz, A. Chuchmała, L. Gorecki, B. A.Sikora, G. Mazurek, Pasciak Opto(electrical) properties of new aromatic polyazomethines with fluorene moieties in the main chain for polymeric photovoltaic devices, Synth. Met. 162 (2012) 143–153.
[25] A. Iwan, B. Boharewicz, I. Tazbir, M. Malinowski, M. Filapek, T. Kłąb, B. Luszczynska, I. Glowacki, K.P. Korona, M. Kaminska, J. Wojtkiewicz, M. Lewandowska, A. Hreniak, New environmentally friendly polyazomethines with thiophene rings for polymer solar cells, Sol. Energy 117 (2015) 246–259.
[26] A. Iwan, E. Schab-Balcerzak, K.P. Korona, S. Grankowska, M. Kamińska, Investigation of optical and electrical properties of new aromatic polyazomethine with thiophene and cardo moieties towards application in organic solar cells, Synth. Met. 185–186 (17–24) (2013).
[27] A. Iwan, B. Boharewicz, K. Parafiniuk, I. Tazbir, L. Gorecki, A. Sikora, M. Filapek, E. Schab-Balcerzak, New air-stable aromatic polyazomethines with triphenylamine or phenylenevinylene moieties towards photovoltaic application, Synth. Met. 195 (2014) 341–349.
[28] A. Iwan, M. Palewicz, A. Chuchmała, A. Sikora, L. Gorecki, D. Sek, Opto(electrical) properties of triphenylamine based polyazomethine and its blend with [6, 6]-phenyl C_{61} butyric acid methyl ester, High Perform. Polym. 25 (2013) 832–842.
[29] A. Bolduc, S. Barik, M.R. Lenze, K. Meerholz, W.G. Skene, Polythiophenoazomethines-alternate photoactive materials for organic photovoltaics, J. Mater. Chem. A 2 (2014) 15620–15626.
[30] A. Iwan, B. Boharewicz, I. Tazbir, M. Filapek, Enhanced power conversion efficiency in bulk heterojunction solar cell based on new polyazomethine with vinylene moieties and [6, 6]-phenyl C_{61} butyric acid methyl ester by adding 10-camphorsulfonic acid, Electrochim. Acta 159 (2015) 81–92.
[31] J.C. Hindson, B. Ulgut, R.H. Friend, N.C. Greenham, B. Norder, A. Kotlewski, T.J. Dingemans, All-aromatic liquid crystal triphenylamine-based poly(azomethine)s as hole transport materials for opto-electronic applications, J. Mater. Chem. 20 (2010) 937–944.
[32] A. Iwan, B. Boharewicz, I. Tazbir, A. Sikora, M. Maliński, Ł. Chrobak, W. Madej, Laser beam induced current technique of polymer solar cells based on new poly(azomethine) or poly(3-hexylthiophene), Chem. Sci. Rev. Lett. 4 (2015) 597–608.
[33] K.P. Korona, T. Korona, D. Rutkowska-Zbik, S. Grankowska-Ciechanowicz, A. Iwan, M. Kamińska, Polyazomethine as a component of solar cells – theoretical and optical study, J. Phys. Chem. Solids 86 (2015) 186–193.
[34] A. Iwan, An overview of LC polyazomethines with aliphatic-aromatic moieties: thermal, optical, electrical and photovoltaic properties, Renew. Sustain. Energy Rev. 52 (2015) 65–79.
[35] A. Iwan, B. Boharewicz, I. Tazbir, M. Filapek, K.P. Korona, P. Wróbel, T. Stefaniuk, A. Ciesielski, J. Wojtkiewicz, A.A. Wronkowska, A. Wronkowski, B. Zboromirska-Wnukiewicz, S. Grankowska-Ciechanowicz, M. Kaminska, T. Szoplik, How do 10-camphorsulfonic acid, silver or aluminum nanoparticles influence optical, electrochemical, electrochromic and photovoltaic properties of air and thermally stable triphenylamine-based polyazomethine with carbazole moieties? Electrochim. Acta 185 (2015) 198–210.
[36] A. Iwan, M. Palewicz, I. Tazbir, B. Boharewicz, R. Pietruszka, M. Filapek, J. Wojtkiewicz, B. S.Witkowski, F. Granek, M. Godlewski, Influence of ZnO:Al, MoO_3 and PEDOT:PSS on efficiency in standard and inverted polymer solar cells based on polyazomethine and poly(3-hexylthiophene), Electrochim. Acta 191 (2016) 784–794.
[37] S. Grankowska Ciechanowicz, K.P. Korona, A. Wolos, A. Drabinska, A. Iwan, I. Tazbir, J. Wojtkiewicz, M. Kaminska, Towards better efficiency of air-stable polyazomethine-based organic solar cells using time-resolved photoluminescence and light-induced electron spin resonance as verification methods, J. Phys. Chem. Part C 120 (2016) 11415–11425.
[38] S. Constantinos, M. Christos, K. Mercouri, Semiconducting tin and lead iodide perovskites with organic cations: phase transitions, high mobilites and near-infrared photoluminescent properties, Inorg. Chem. 52 (2013) 9019–9038.
[39] J.H. Heo, S.H. Im, J.H. Noh, T.N. Mandal, Ch.-S. Lim, J.A. Chang, Y.H. Lee, H.-J. Kim, A. Sarkar, Md. K. Nazeeruddin, M. Grätzel, S.I. Seok, Efficient inorganic-organic hybrid heterojunction solar cells containing perovskite compound and polymeric hole conductors, Nat. Photonics 7 (2013) 486–491.